Available online at www.sciencedirect.com
ScienceDirect
Advances in Space Research 48 (2011) 1359–1370
ADVANCES IN SPACE RESEARCH (a COSPAR publication)
www.elsevier.com/locate/asr

Gravity wave momentum flux generation close to mid-latitude Andes in mesoscale simulations of late 20th and 21st centuries

P. Alexander [a,*], R. Ruscica [b], A.A. Sörensson [b], C.G. Menéndez [b,c]

[a] Departamento de Física, Facultad de Ciencias Exactas y Naturales, Universidad de Buenos Aires, 1428 Buenos Aires, Argentina
[b] Centro de Investigaciones del Mar y la Atmósfera, Facultad de Ciencias Exactas y Naturales, Universidad de Buenos Aires, 1428 Buenos Aires, Argentina
[c] Departamento de Ciencias de la Atmósfera y los Océanos, Facultad de Ciencias Exactas y Naturales, Universidad de Buenos Aires, 1428 Buenos Aires, Argentina

Received 6 October 2010; received in revised form 23 May 2011; accepted 24 June 2011
Available online 1 July 2011

Abstract

Adequate representations of diverse dynamical processes in general circulation models (GCM) are necessary to obtain reliable simulations of the present and the future. The parameterization of orographic gravity wave drag (GWD) is one of the critical components of GCM. It is therefore convenient to evaluate whether standard orographic GWD parameterizations are appropriate. One alternative is to study the generation of gravity waves (GW) with horizontal resolutions that are higher than those used in current GCM simulations. Here we assess the seasonal pattern of topographic GW momentum flux (GWMF) generation for the late 20th and 21st centuries in a downscaling using the Rossby Centre regional atmospheric model under the Intergovernmental Panel on Climate Change A1B emission conditions. We focus on one of the world's strongest extra-tropical GW zones, the Andes Mountains at mid-latitudes in the Southern Hemisphere. The presence of two GCM sub-grid scale structures locally contributing to GWMF (one positive and one negative) is found to the East of the mountains. For the late 21st century the strength of these structures during the GW high season increases around 23% with respect to the late 20th century, but the GWMF average over GCM grid cell scales remains negative and nearly constant around −0.015 Pa. This constitutes a steady significant contribution during GW high season, which is not related to the GWMF released by individual sporadic strong GW events. This characteristic agrees with the fact that no statistically significant variation in GWMF at source level has been observed in recent GCM simulations of atmospheric change induced by increases in greenhouse gases.

Keywords: Gravity waves; Momentum; Numerical simulations

1. Introduction

A broad spectrum of waves transports momentum in the atmosphere. Among the ones that exhibit small scale on the horizontal plane (wavelengths ranging from approximately 10–1000 km) are the so called gravity waves (GW), which are generally unresolved or poorly represented in general circulation models (GCM). However, it is well-known that these waves have significant effects on the general circulation, temperature structure, and chemistry of the middle atmosphere (e.g., Eyring et al., 2007; Fritts and Alexander, 2003; Lindzen, 1973; Walterscheid, 2001). Despite their small scale and local presence, their collective effects are seen on planetary distances. The deployment of high-resolution measurements from space in the last 15 years allowed an improvement in the global description of GW (e.g., Eckermann and Preusse, 1999; Fetzer and Gille, 1994; Preusse et al., 2000, 2008; Tsuda et al., 2000; Wu and Waters, 1996; Wu, 2004; Wu et al., 2006).

The absorption or dissipation of GW produces significant body forces on the atmospheric flow, known as gravity wave drag (GWD). A GCM with extremely high resolution would be required to simulate the full spectrum of small scale GW that produce the GWD. Presently, and probably not in the near future, this is not feasible, so the

* Corresponding author.
E-mail address: peter@df.uba.ar (P. Alexander).

0273-1177/$36.00 © 2011 COSPAR. Published by Elsevier Ltd. All rights reserved.
doi:10.1016/j.asr.2011.06.020

effects of the non-resolved GW must be represented in a parameterization, which is a critical component of the models (e.g., Kim et al., 2003). GWD parameterizations are currently acknowledged to perform barely adequately at best. However, they will need to capture adequate sensitivity to atmospheric changes induced by climate change in order to obtain reliable simulations of the future. If present and future GW sources, propagation and dissipation could be more realistically characterized in model experiments, then an important obstacle to accurate parameterizations would be reduced. However, required information would include for example horizontal wavelengths and spatial and/or temporal frequency of the generated GW. Since there is not yet an established method to describe a GW source and propagation spectrum from a numerically resolved circulation, it is necessary to specify these aspects externally. Various poorly constrained parameters that describe wave properties are then set. For example space and time constant GW parameters are often used (e.g., Fritts and Alexander, 2003). Even if this choice of parameters could be considered acceptable for the current GW spectrum, the future excitation characteristics might require modifications on prescribed wavelength, amplitudes and assumptions on spatial and temporal homogeneity and isotropy of the source spectrum, as they may be functions of changing climate parameters.

GW from non-orographic sources, if included at all in GCM, are input with time constant or globally uniform properties or that vary only as a function of latitude. None of the GCM in the last report from the Intergovernmental Panel on Climate Change (IPCC) include non-orographic GWD parameterizations. GW generated by flow over topography are assumed to be stationary with respect to the ground in GCM parameterizations (e.g., Hong et al., 2008; Lott and Miller, 1997; McFarlane, 1987; Palmer et al., 1986; Scinocca and McFarlane, 2000; Webster et al., 2003). Time varying flow over orography can generate non-stationary waves, but these are ignored for simplicity. However, Chen et al. (2005) have shown that even very slow flow evolution has a major impact on the momentum flux. At the present time there is a consensus that orographic and non-orographic GWD parameterizations need significant improvements. For example, to make the problem tractable and computationally efficient, important simplifying assumptions are currently made about the physics and computation of the generation, propagation and dissipation of GW. It is usually considered that the GW propagate only vertically and instantly through a column. Energy flux is conserved up to a height at which a wave amplitude limit has been reached, so at larger heights breaking and momentum flux deposition occur, which generates the GWD. All parameterizations use adjustable parameters to tune the wave drag and the breaking heights. The parameter values should be constrained by observations, but these are still insufficient. Then, parameters are usually determined by tuning the model results to observed climatologies. This leads to miss some important although infrequent behaviors observed in variables by reliable instruments (Lovejoy et al., 2009).

Although possible consequences of global atmospheric change do not only apply to tropospheric weather and climate but also to the dynamics of the lower and middle atmosphere, a very small fraction of the simulations literature for the future focuses on the latter subject. One exception is the recent coincident result in at least three independent models (Garcia and Randel, 2008; Li et al., 2008; McLandress and Shepherd, 2009): in the long-term, variations in parameterized orographic GWD would be driving changes in the strength of the Brewer–Dobson circulation. This happens through an indirect chain, where variations in extra-tropical winds due to orographic GWD change the refraction and breaking characteristics of planetary waves, thereby affecting the extra-tropical input to the Brewer–Dobson circulation. The composition of the stratosphere, particularly its water vapor content, has important consequences for climate (see, e.g., Forster and Shine, 2002; Solomon et al., 2010).

The difficulties of orographic GWD parameterizations in helping to reproduce present conditions in GCM are well-known. As GCM response may be sensitive to parameterized orographic GWD settings, it may lead to non-robust aspects, whereby subtle changes might confuse the interpretation of simulated results of the future. In addition, the response of GWD parameterizations to CO_2 forcing could be highly dependent on the parameter values. Climate simulations that include the greenhouse gas evolution by Sigmond et al. (2008) exhibited a clear sensitivity of zonal wind strength in the mid- and high-latitude lower stratosphere and mean sea-level pressure to orographic GWD (this was later re-evaluated and minimized by Sigmond and Scinocca (2010)). A possible scenario could be that a change in the vertical temperature structure of the atmosphere due to a change in CO_2 concentration may cause changes to the dynamics, for example in the generation of GW in the lower atmosphere and their propagation in the middle atmosphere (e.g., Rind et al., 1990). Any change in the circulation arising from a change in GW forcing could then further modify the temperature structure. For this reason, the type of scheme or parameter values that are used may play an important role in the modeled response to a change in the CO_2 concentration. It follows that the representation of orographic GWD could be recognized as a very critical gear part in GCM. It is not the aim of this work to study the details of the CO_2 – GW feedback mechanism, but to provide results that may be used to evaluate if the available GWD parameterizations are adequate for present and future conditions. Studies have usually not considered the possible need of adjustment or change of those representations in an evolving atmosphere. May present representations of GWD become even less appropriate for simulations affected by global atmospheric change, as the numerical results can only be tuned and compared to present climatologies? If so, this would add further uncertainties to the usually recognized ones for

GCM projections. One alternative in order to test GWD parameterizations is to analyze the present and future GW scenarios under higher horizontal resolution simulations. The three basic components of GWD parameterizations are (i) the characteristics of the source, (ii) wave propagation and evolution as a function of height and (iii) wave dissipation and the effects on the background atmosphere. It is the confidence of the source description of orographic GWD parameterizations that is relevant for the present work.

GCM do not only have a too low resolution to correctly represent the GW spectrum, but they also have problems in dealing with high and sharp topography. In addition they have difficulties in accurately computing the pressure interaction term near orography (see, e.g., Lappen and Randall, 2001). Regional climate models (RCM) with large domains are now being routinely used at high enough horizontal resolutions for GW to become at least partially resolved. GWD parameterizations, which are simplified process representations in absence of more adequate computationally cheap options, are therefore not as essential in RCM. Below we use a GCM to initialize and drive a RCM, which has a horizontal resolution that allows to resolve a significant part of GW and topography issues. We study simulations of the present and the future of one of the world's extra-tropical strongest sources of GW, the Andes Mountains at mid-latitudes in the Southern Hemisphere (de la Torre and Alexander, 2005; Eckermann and Preusse, 1999). The scenario resembles a two-dimensional (2D) configuration, where a North–South topographic barrier acts on the intense prevailing zonal winds blowing from the Pacific Ocean in the lower troposphere. Large amplitude GW are generated by this forcing mechanism.

This work addresses the generation of GW momentum flux (GWMF) by orography under present and predicted future atmospheric conditions. Two series of twenty year RCM simulations (one for the present and one for the future) close to a well-known source of GW are analyzed from the point of view of generation of resolved-scale features. This study focuses on the reliability of the source description of the orographic GWD parameterizations in GCM, as recent literature shows that model results may be sensitive to the schemes that have been implemented inside them. A horizontally higher resolution RCM may explicitly without parameterizations represent small-scale GW and the related momentum flux extracted from the results. Then, the representativeness of the parameterized GWD in GCM could be evaluated in present and future scenarios.

2. The regional model experiment

A small amount of high resolution scenarios are up to this date available for South America using RCM driven by coupled atmosphere ocean GCM (AOGCM) and given emission scenarios. Almost all of them have time spans no longer than 10 years (we are only aware of Marengo et al. (2009) with 30 year intervals). In this study we examine RCM simulations carried out over the South American continent with the most recent version of the Rossby Centre regional atmospheric model RCA3 (Kjellström et al., 2005). The model domain is based on a rotated grid system with a horizontal resolution of 0.5° (roughly 50 km at mid-latitudes) and 24 unevenly spaced sigma levels in the vertical, whereby the lid is at 10 hPa. The Max Planck Institute coupled AOGCM ECHAM5/MPI-OM (Jungclaus et al., 2006) was used to initialize and drive a continental scale RCA3 domain for the present and the future. To assess the model performance, "perfect" boundary conditions were employed by nesting the RCM in the European Center for Medium-Range Weather Forecasting reanalysis dataset ERA40, which has a horizontal resolution of 2.5°, for the period 1980–1999 (this simulation will hereafter be called RCAERA). The periods 1980–1999 (present, hereafter RCA20) and 2080–2099 (future, hereafter RCA21) were simulated. Years 1979 and 2079 were respectively used for spin-up of the RCA20 and RCA21 simulations. The radiative forcing of the system is based on 20C3M, a scheme with historical greenhouse gas concentrations, and on the IPCC A1B emission scenario for the present and future respectively. The difference between RCA20 and RCAERA simulations is interpreted as the error introduced by the AOGCM. The difference between RCA21 and RCA20 simulations is defined as the response of the RCM to the A1B scenario. These simulations have already been used to project climate changes in South America (Sörensson et al., 2010).

It must be stated that every climate model has limited credibility in the medium and long term. This follows from the well-known fact that operational forecast models with an order of magnitude better spatial resolution and constrained by near real time observations run out of skill in less than ten days. In addition, the one way nested RCM domain in our numerical runs might limit certain feedbacks such as synoptic or planetary wave – GW interactions. The former waves have typical horizontal wavelengths of some 1000 km or larger and are included in the RCM through the boundary conditions. However, there is no feedback between the GWs generated by the RCM and the GCM planetary or synoptic waves. As an example of this type of mechanism, Sigmond and Scinocca (2010) found that the influence of orographic GW response to climate change in the simulated Northern Hemisphere circulation was indirect and associated with determining differences in the planetary wave propagation characteristics.

3. Simulation results

Vertical velocity variation and quasi-stationary ground-based horizontal phase velocity are recognized as strong indicators of the presence of GW due to topography (e.g., Baines, 1995; Shutts et al., 1988). The highest Andes tops reach almost 7000 m height (about 400 hPa), so we decided to perform our waves survey just above, at the

300 hPa level. This represents an altitude of approximately 10 km, which is an acceptable source height from the point of view of stratospheric dynamics. GW amplitudes increase with height (e.g., Hines, 1960), so it would seem a priori more appropriate to perform the analysis at a higher level, as the waves would be more clearly observed. However, they could be absorbed, break, dissipate or become trapped in their propagation upwards (Fritts and Alexander, 2003) and then they might not be observed at all in a study made at higher altitudes.

Fig. 1 exhibits the topography and the mean over 20 winters (this season is shown as an example) of horizontal wind to the West of the Andes mountains at 500 hPa according to RCA20, giving a nearly 2D scenario. The horizontal wavefronts of the GW generated by this kind of configuration are expected to essentially lie along the N–S direction (e.g., Baines, 1995). In Fig. 2a we exhibit pressure coordinate vertical velocity over South America at 300 hPa for RCA20. For general assessment of the error generated by the boundary conditions of the AOGCM we also include in Fig. 2b RCAERA. Similar large scale patterns may be observed over the continent for both simulations during all seasons (summer (DJF), autumn (MAM), winter (JJA) and spring (SON)). Permanent wavy structures over the Andes become evident at mid-latitudes and are strongest in winter and spring, which is in agreement with observations (e.g., Alexander et al., 2010). We also notice that the phase of the mountain waves structure

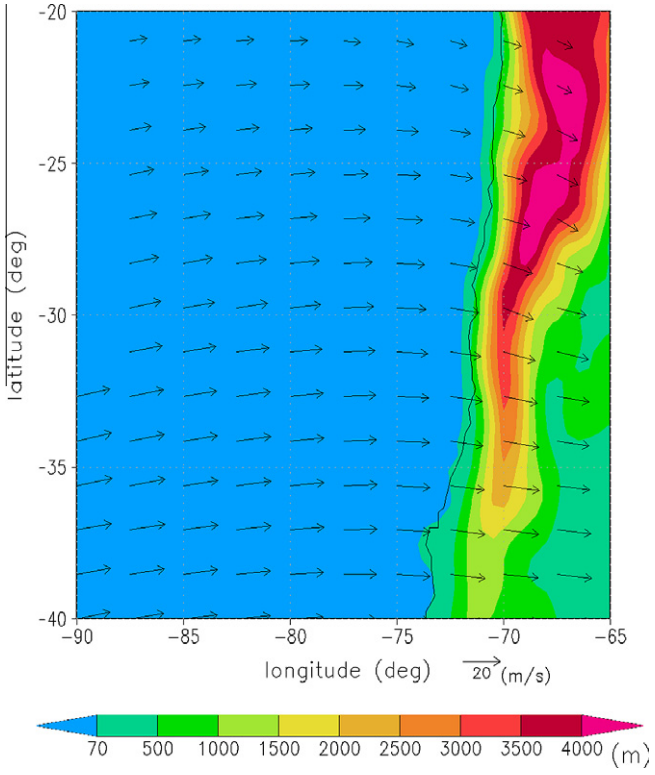

Fig. 1. The topography and the mean horizontal wind over 20 winters simulated by RCA20 to the West of the Andes mountains at 500 hPa. The extension of the shading into the ocean in some places is an artifact of the interpolation used in the plotting software.

is stationary: there is no displacement with season and the standard deviation of the mean is much smaller than the average value shown in each point (see Fig. 2a and c). When zooming in on the data, some spatially and temporally located strong GW events may be found mainly in winter and spring which, however, being sporadic do not add significantly to the overall standard deviation or mean. In Fig. 3 we show the monthly means over the 20 years of the zonal wind blowing at 30S from the West at 500 hPa called $U500$, just above Andes (meridional wind is usually much smaller, see Fig. 1). The behavior is representative of the upstream zonal wind at mid-latitudes that grazes the Andes tops. It may be clearly seen that the strongest values may be found during winter and spring, in coincidence with the largest wave amplitudes. Notice also that RCA21 predicts stronger zonal winds with respect to RCA20 over all the months. The larger winds imply a stronger forcing and a lower probability of finding critical levels where GW could be absorbed (i.e., zero wind zones for nearly stationary mountain waves as seen from the ground) and larger saturation wave amplitudes (Alexander, 1998). There is in addition a statistically significant change in stability at the 90% level in the simulations, where the average Brunt–Väisälä frequency in the lower troposphere rises by about 7% for JJA and 5% for SON between RCA20 and RCA21.

The GWMF τ is equivalent to the rate per unit area at which horizontal momentum is being transferred vertically by the waves (Gill, 1982). The lack of observational constraints for orographic GWMF close to source altitudes implies that uncertainties about its generation in GCM cannot be evaluated, so any further information about expected values may be useful to find adequate schemes for the present and the future. In order to estimate τ due to the generation of GW by Andes at mid-latitudes we must calculate from our simulations

$$\tau = \bar{\rho}\overline{uw} \tag{1}$$

where $\overline{uw}$ represents a horizontal average of the product of zonal and vertical velocity wave components over a representative scale, whereby $\bar{\rho}$ is the background density (Andrews et al., 1987). The horizontal average may be performed on a surface on the order of a GCM grid scale (Fritts and Alexander, 2003). Negative τ means an upward flux of negative momentum or a downward flux of positive momentum. In Fig. 4 we see $U300$ and $\Omega 300$ corresponding to the seasonal zonal and pressure coordinate vertical velocity profiles against longitude at 30S and 300 hPa for RCA20 and RCA21 (uncertainties bands correspond to the standard deviation of the mean). A zonal wavelength footprint around 530 km may be found in all panels (at 30S 1° longitude represents about 96 km). Waves with zonal scales on the order of a few 100 km may then be a significant contributing factor for GWMF. Shorter wavelengths are expected to have smaller amplitudes according to the power law between saturation amplitudes and horizontal wave numbers for scales up to about 100 km (Bacmeister et al., 1996). The

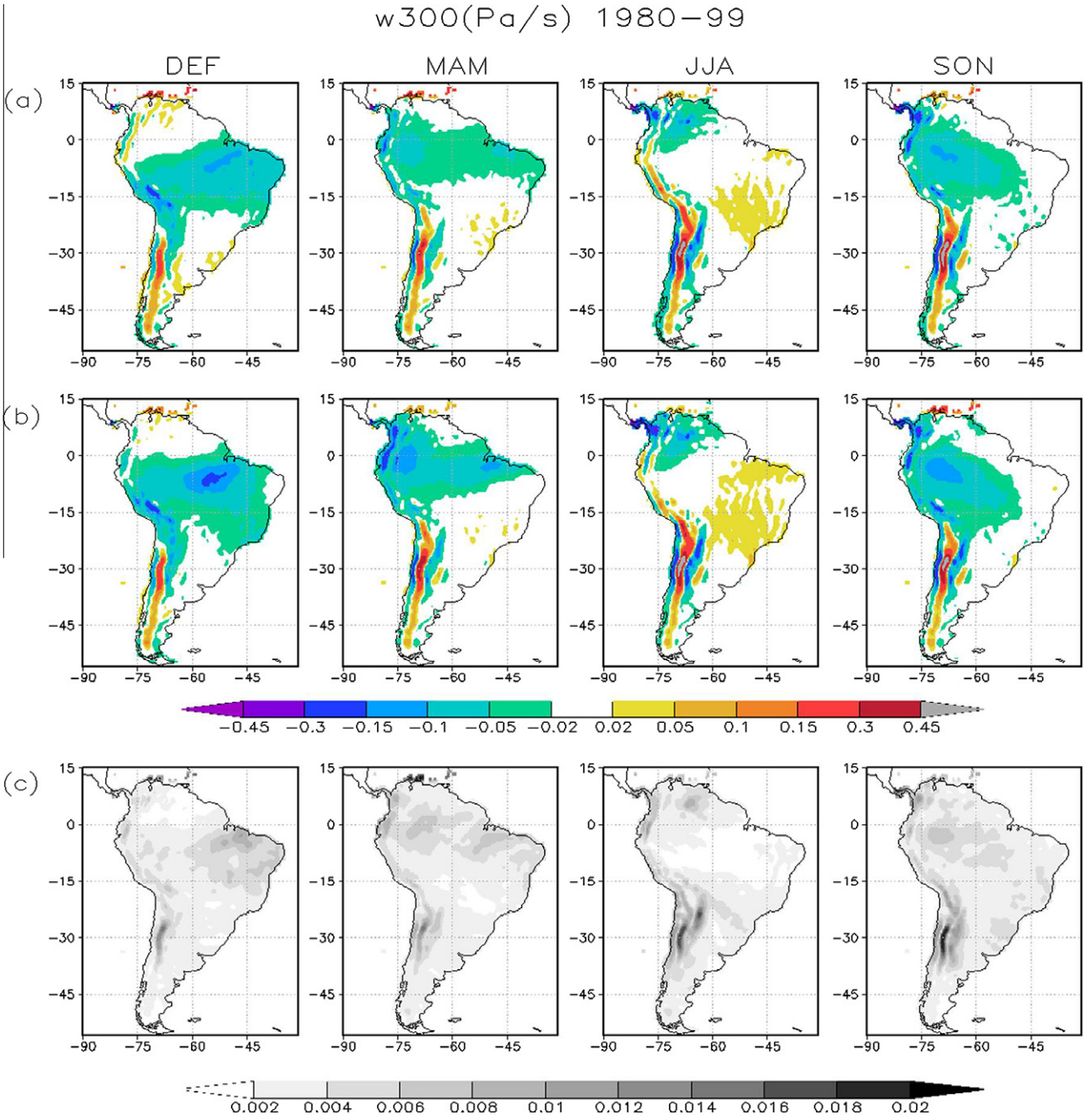

Fig. 2. Pressure coordinate vertical velocity (1 Pa $s^{-1} \approx -0.23$ m s^{-1}) per season over South America at 300 hPa for simulations: (a) RCA20, (b) RCAERA and (c) the standard deviation of the mean for RCA20. Horizontal and vertical axes respectively show longitude and latitude (in degrees).

velocity is now decomposed into background (U, W) plus wave components (u, w). There is no unique background removal method and each of them has advantages and drawbacks in the outcome (e.g., Zülicke and Peters, 2006). The background zonal velocity at 300 hPa for each time step of the solution has here been obtained at each latitude from the longitudinal profile after removal of the variations on scales less than 1000 km. The digital filter applied is nonrecursive and to avoid Gibbs effects a Kaiser window was used (e.g., Hamming, 1998). The horizontal and vertical wave components u and w may then be calculated from the simulated and background velocities in each grid cell at each time step. The background vertical velocity at 300 hPa is taken null $(W = 0)$ for all time steps. Density has been obtained from the model simulations. In Fig. 5 we show the RCA20 and RCA21 zonal velocity background profiles averaged over 20 years for each season at 300 hPa and 30S latitude (compare with Fig. 4) as a representation of typical conditions where individual GW events are immersed.

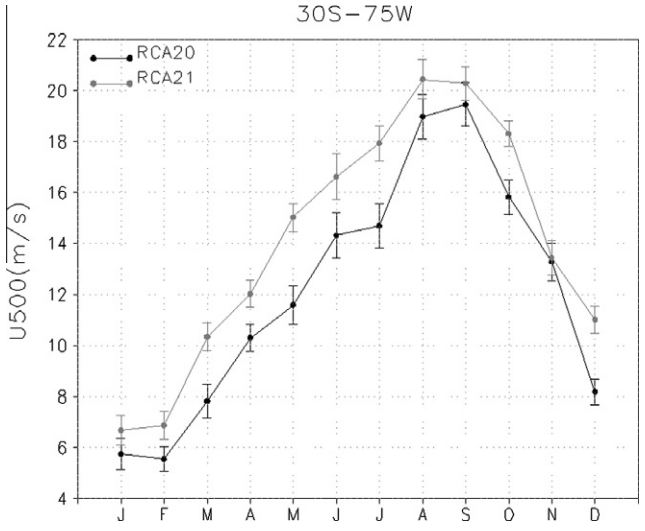

Fig. 3. Monthly means of the zonal wind at 500 hPa blowing from the West of the mountains at 30S for RCA20 and RCA21.

4. Discussion

We see in Fig. 6 a decomposition in terms of local contributions to the total GWMF generated by the topographic source in the studied area. It is a 20 years average horizontal distribution at 300 hPa for respectively RCA20 and RCA21 simulations in terms of season. Highest absolute values are found during winter. This applies to the black and white sectors in the middle of the panels, which represent areas of extreme negative and positive contributions to GWMF respectively. Increases in the averages for these regions between RCA20 and RCA21 during JJA and SON are shown in Table 1 and they are statistically significant at the 90% level. The average contribution to GWMF in both strong areas rises around 23% for each season and sign. A uniform and constant upstream flow over sinusoidal terrain would create linear GW that generate everywhere a strictly negative contribution to τ (Nappo, 2002). The simulated situation is a more complex one and the outcome is the generation of two neighbor areas, which have respectively significant positive and negative GWMF contributions during JJA and SON. During MAM both regions become mild, whereas they are almost unseen for DJF. Negative areas are somewhat larger than positive ones. For JJA and SON these structures possess areas smaller than 40,000 km^2, which is representative of GCM grid cells. These models usually have a horizontal resolution coarser than 100 km (for example those used in the last report of the IPCC range between 125 km and 400 km), so they cannot clearly resolve the GW observed in this study and the structures that they may create. The average GWMF over the whole square of this study (around 4,000,00 km^2) is nearly the same during JJA and SON for RCA20 and RCA21 (around -0.015 Pa for winter and spring in both centuries). This is a kind of steady contribution during both seasons but is not related to the GWMF released by individual strong sporadic GW events. It should be also remarked that the general background for JJA at RCA21 looks quite different than in the other cases, but the corresponding values are nevertheless not significant as compared with the black or white areas.

The presence of one negative but particularly also of one positive contribution to GWMF deserves an interpretation. As we are dealing with an orographic source, one would expect to observe upward propagating waves with negative GWMF that decelerate the mean flow. Notice that the cross-correlation term does not change sign even if the mean zonal wind does. Positive GWMF could mean downward propagating waves, which would be possible if there was above 10 km in the model (i) a non-orographic stationary source of downwelling GW or (ii) a stationary reflection level of GW, or if (iii) Eq. (1) and/or the model output and/or the separation between background and perturbation are not suitable or accurate enough to describe the resolved GWMF. Alternative (i) is very unlikely. Option (ii) could be due to an upper boundary formulation problem of the numerical model, whereby the resolved waves would be reflected from the top layers or from the above and close tropopause or from a horizontal wind maximum level. In relation to (iii), the absorption or breaking of the GW created by the model into turbulence may not be correctly described by the turbulence parameterizations of the RCM. However, patterns of waves in longitude–vertical cross sections retain phase lines that are tilted in the appropriate direction, corresponding to upward propagation (against the background flow), hence there is no superposition of an upward and a downward propagating wave or a strange behavior. After discarding the above true possibilities or artifacts we look for a possible interpretation of the positive contribution to GWMF. For the cross-correlation term $\overline{uw}$ to be physically representative, it must be averaged over a meaningful horizontal scale (Nappo, 2002), e.g., the horizontal wavelength of the most significant generated waves ($\sim$500 km, which is somewhat larger than typical GCM grid point separations). The important fact is that the sum of the GWMF contributions of both zones remains negative. Any deviation from a horizontally uniform negative GWMF reflects a departure from a uniform and constant horizontal wind over a small sinusoidal corrugation scenario, because the polarization relations change with respect to zonal and vertical velocity perturbations being exactly out of phase. All these aspects refer to lee phenomena, as there are no clear upstream effects on GWMF as observed at 300 hPa. Bacmeister et al. (1990) already suggested that the GWMF value from flow over large 2D ridges is similar to the amount generated by an obstacle of a height on the order of the ratio of the upstream speed and the Brunt–Väisälä frequency (about 1 km for typical tropospheric conditions). This obstacle height represents the threshold where upstream partial blocking begins to occur.

GCM ECHAM5 is consistent with the observed seasonal behavior in τ in the present study: GWD per unit area at the source level is represented as being proportional

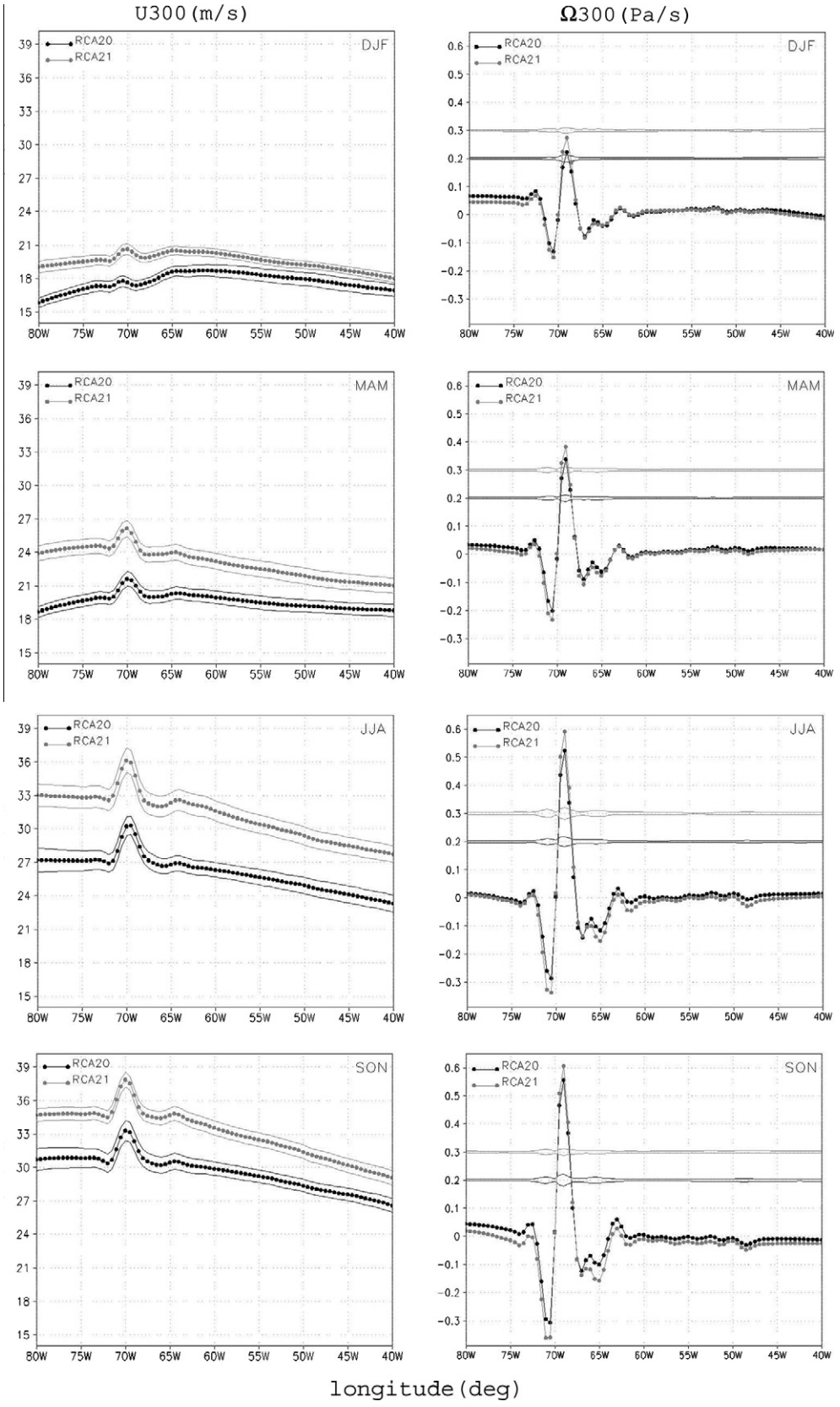

Fig. 4. The seasonal zonal and pressure coordinate vertical wind profiles at 300 hPa height and 30S latitude against longitude for RCA20 and RCA21 ($1\ \mathrm{Pa\ s^{-1}} \approx -0.23\ \mathrm{m\ s^{-1}}$). Bands represent uncertainties determined by the standard deviation of mean. For better visibility the pressure coordinate vertical wind uncertainty bands have been centered at 0.2 and 0.3 $\mathrm{Pa\ s^{-1}}$, respectively for RCA20 and RCA21.

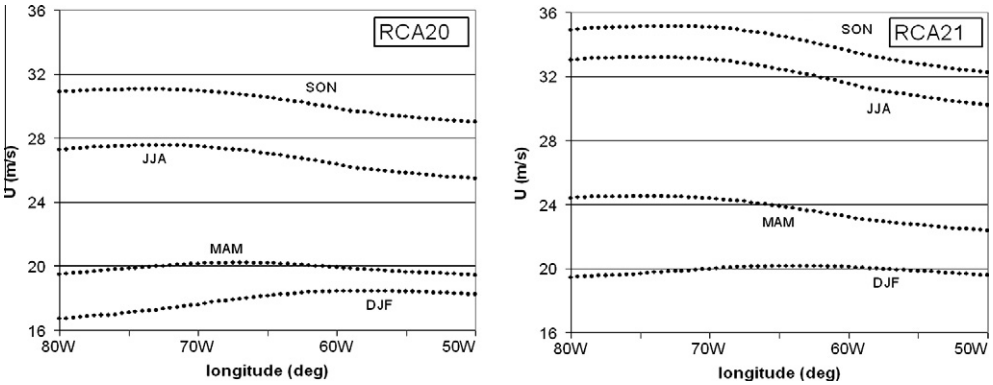

Fig. 5. Background zonal velocity averaged over 20 years per season at 300 hPa height and 30S latitude for RCA20 and RCA21.

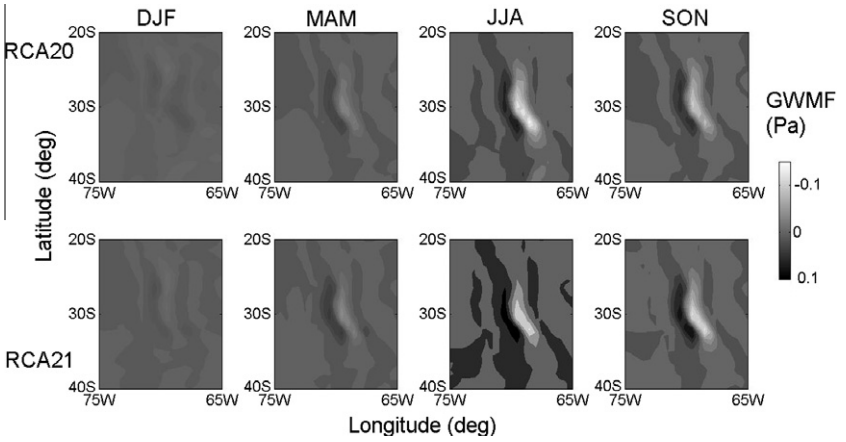

Fig. 6. Horizontal distribution at 300 hPa of local contributions to average GWMF over the 20 years of respectively RCA20 and RCA21 simulations in terms of season.

Table 1
Average contributions to GWMF (Pa) in the regions of extreme positive/negative values.

	*RCA*20 (Pa)	RCA21 (Pa)
JJA	0.061/−0.113	0.075/−0.139
SON	0.052/−0.101	0.064/−0.124

to the magnitude of the incident flow at mountain heights (Roeckner et al., 2003), whereby spring and winter are the most intense westerly seasons at mid-latitude Andes heights according to RCA20 and RCA21 zonal velocity profiles in Fig. 3. Also, when comparing RCA21 with respect to RCA20, higher values of the zonal wind at mountain heights and larger contributions to τ (Fig. 6) both occur in the simulation of the future.

About 10–20% stronger zonal winds and a 5–7% increase in stability in the lower troposphere are anticipated with 90% statistical significance for the 21st century during winter and spring. Stronger wave activity may be expected for the late 21st century, because it was noticed above that a larger horizontal wind may produce that effect. In addition, the higher stability leads to the possibility of generating larger wave amplitudes. As a consequence, the strength of GWMF released by the Andes source at mid-latitudes in the Southern Hemisphere during winter and spring could rise.

The generated GW structure and the amount of launch momentum due to the interaction of the circulation and topography in a 2D picture (like Andes at mid-latitudes) essentially depends on two non-dimensional parameters (Baines, 1995; Nappo, 2002; Pierrehumbert and Wyman, 1985; Rontu, 2007; Stein, 1992): $A = Nb/U$ and $F = Nh/U$, N and U being respectively the upstream Brunt–Väisälä frequency and zonal velocity, whereby b corresponds to the half-width of the obstacle at mid-height of top altitude h. The former parameter represents a non-dimensional half-width of the obstacle and evaluates the hydrostatic degree of the problem (large values correspond to the hydrostatic limit). Being larger than one it ensures that the generated horizontal wavelengths are not shorter than the minimum required by the Scorer parameter to propagate without evanescence. The other value represents a non-dimensional height of the ridge and it controls the non-linearities (the regime out of linearity is achieved above values around 1). It corresponds to an inverse Froude number which also allows evaluation of whether the incoming flow energy is sufficient to overcome the topographic obstacle or if a

Table 2
Seasonal values of non-dimensional numbers characterizing GWMF generation and their uncertainty due to inter-annual variability.

	A (RCA20/RCA21)	F (RCA20/RCA21)	B (RCA20/RCA21) (%)
DJF	43.5/35.5	7.0/5.7	±8.9/7.3
MAM	27.4/23.1	4.4/3.7	±7.1/4.9
JJA	16.4/15.5	2.6/2.5	±6.1/5.1
SON	16.7/16.5	2.7/2.6	±5.3/4.2

fraction becomes blocked. Onset of blocking has been found around a value of 2. Coriolis effects are neglected here because a typical zonal wind speed $U = 10\ \mathrm{m\ s^{-1}}$ for a 100 km wide range implies a time to traverse it that is less than 3 h, whereas the Coriolis parameter at these latitudes is associated to a 1 day period. The absence of rotation effects ensures that the problem can be approximately considered 2D. Representative values for Andes at mid-latitudes are $b = 25$ km and $h = 4$ km (see Fig. 1).

In Table 2 we show the parameter values in the upstream region for every season according to RCA20 and RCA21 simulations. Associated uncertainties at the seasonal scales are related to the confidence bands of N and U, where the latter quantity plays the key role. Uncertainty B in Table 2 stems from the simulated inter-annual seasonal variabilities in the upstream region estimated by the standard deviation of the mean. Other possible uncertainties in the same zone respectively come from the RCM performance (evaluated by comparing RCAERA against ERA40) and biases introduced by the AOGCM boundary conditions (estimated from the difference between RCA20 and RCAERA). The former exhibits overestimations which are very similar to the RCA20 magnitude of B, whereas the latter leads to underestimations that are twice as large during DJF and MAM, negligible during JJA and four times as large overestimation during SON. It follows that a remarkable aspect is the significant error introduced by the AOGCM boundary conditions during spring. This is mainly caused by a 22% excess in RCA20 upstream zonal velocity with respect to RCAERA values. It should be also taken into account that the non-dimensional number calculations assume uniform and constant upstream variables and 2D configuration, which are reasonable simplifications of complex phenomena, but they suit to some degree of accuracy the real or simulated conditions. In controlled laboratory experiments it may be possible to more closely approach the assumed characteristics (see, e.g., Baines (1995)).

After the above evaluations, we may extract some general conclusions from the evolution of non-dimensional numbers, but strict compliance of typical regimes with numbers is not expected. F shows that the waves stay in the non-linear regime or close to the critical transition to it. During winter and spring the F values show an approach to the linear behavior, where waves may propagate vertically. Although GW horizontal wavelength may range from a few tens to several hundred kilometers in the studied region (e.g., de la Torre et al., 2009), only very large wavelengths (around 500 km) have a constructive pattern over time that leaves a permanent footprint according to the above simulations. In the true atmosphere the smaller scale waves probably exhibit a tendency to disappear after a few hours or days due to flow blocking and wave breaking, that occurs when $F \geqslant 2$ (e.g., Rontu, 2007) and therefore being so infrequent may have a tiny effect in long term averages. Seasonal mean biases of RCA20 are larger in magnitude than the differences with RCA21. Then, more favorable conditions for the generation of GW during the 21st century as concluded from parameter F are not statistically significant. This applies very clearly for JJA and SON, which are the most intense seasons. However, the same evolution in terms of season may be expected along both centuries for F, that is to say for GW intensity.

A in Table 2 corresponds to hydrostatic waves. A study of GWD in terms of A for a linear flow regime over a small bell-shaped hill (Gill, 1982) deviates from the present conditions but may just aid in the interpretation of results. It is there shown that the GWD (a possible loose proxy for the GWMF) reaches a maximum for $A = 10$ and then decreases for larger values. This is in agreement with the lowest A values (but above 10) and the strongest local GWMF contributions occurring during JJA and SON (see Table 2 and Fig. 6).

According to linear theory the drag per unit length (2D configuration) caused by the pressure difference between the windward and leeward sides due to GW is given by $C\rho NUh^2$ or equivalently by $C\rho FU^2h$, where C is a coefficient around 1 (see, e.g., Smith, 2001). Numerical models like ECHAM5 generally use this estimate for the GWD source term of the unresolved portion of the spectrum. The simulated parameter F changes slightly between centuries for JJA and SON because increases in N and U nearly compensate (as described above). Using the values from Fig. 3 and Table 2 and an obstacle width of 100 km, we obtain a proxy for the source term of GWD in the parameterization schemes over Andes around a few Pa according to RCA20 and RCA21, being about 20% larger for the latter. However, the true surface pressure differences are somewhat smaller because the lowest level flow gets blocked on the upstream side (see the above description of F), so only a fraction of h should be considered in the generation of vertically propagating waves. The long-term horizontal average values over the studied square in Fig. 6 are around -0.015 Pa during GW high season, which is a realistic order of magnitude (see below).

A comparison with measurements of τ would be very useful. However, there are no global measurements that account for the distribution in the troposphere. Such a study has been performed in the stratosphere at 25 km altitude in a one week "snapshot" during August 1997 (Ern et al., 2004). Values of τ of a few mPa have been observed in the region we studied, but zones reaching 50 mPa have been found over the continental southern tip, the Drake Passage and the Antarctic Peninsula, which are the largest global results. All these values give just an order of magnitude reference. There are several reasons that make comparisons difficult. As stated, the measurements stem from just one week. Also, the instrument used is sensitive to the portion of the GW spectrum that possesses horizontal wavelengths larger than about 200 km (Wu et al., 2006). Visibility down to about 100 km wavelengths may be achieved in some cases (Preusse et al., 2002). Also, our numerical study has been performed just above the source, at about 10 km altitude in the troposphere, whereas the global measurements have been obtained at 25 km height, in the stratosphere. GW propagating upwards may dissipate, break, become absorbed or trapped, so only the presence of another source above topography would prevent τ from decreasing with height. Finally, GW events are sporadic (see, e.g., Fritts and Alexander (2003)), so it is difficult to compare long-term averages like in this work with short-term observational studies from a week or so. Ern et al. (2004) found similar challenges and discrepancies in τ values when they tried to compare their results with observations of other instruments in certain regions.

Recent GCM simulations of the response to climate change (e.g., McLandress and Shepherd, 2009; Sigmond and Scinocca, 2010) do only find slight changes in the orographic GWMF at the source level and just a statistically significant vertical shift in GWD is observed. On the other hand, wind and stability characteristics simulated by RCA3 would imply that larger GWMF could be expected for the 21st century. However, after averaging GWMF over the whole area of study (it typically represents a few GCM grid cells), RCA results coincide with the recent GCM simulations, i.e., there is no significant change in the source strength. This happens because although the intensity of positive and negative local contributions to GWMF increases, the mean over the whole studied area during GW high season (JJA and SON) in RCA20 and RCA21 were all nearly identical. In brief, statistically significant changes between RCA20 and RCA21 in local contributions to GWMF are found in GCM sub-grid scales according to the present results (possibly due to the above described statistically more favorable conditions for GW generation). However, the effects compensate and GW source models with no significant change in strength between 20th and 21st centuries may be an appropriate representation in GCM for regions with topography (at least near to southern mid-latitude Andes).

5. Conclusions

The present work uses a better than standard GCM horizontal resolution for late 20th and 21st century simulations over mid-latitude Southern Andes under the A1B emission scenario. It is then able to find on GCM sub-grid scales GWMF local contributions with a permanent structure at source level, with one significantly positive and one significantly negative zone to the East of Andes during winter and spring. This is generated by horizontal wavelengths around 500 km. The shorter scale waves may have smaller amplitudes and be also less frequent, therefore they may have a very small effect in long term momentum averages. A similar seasonal evolution to the present one is expected for GWMF generation in the 21st century. The simulations show that the large positive and negative contributions to GWMF in the studied region would intensify around 23% during winter and spring of the next 100 years. This may be related to the fact that predicted changes led to statistically significant more favorable conditions for GW generation in relation to wind and stability. However, the impact of GWMF averaged over horizontal scales of GCM grid cells stays nearly constant around -0.015 Pa for GW high season in both centuries. This coincides with recent GCM simulations that have not detected a significant future variation in GWMF generation. It must be stated that the nearly steady GWMF during JJA and SON is a permanent contribution during both seasons, but is not related to the amount launched by individual sporadic strong GW events.

The nearly permanent dipole type GWMF configuration could also appear in the neighborhood of other abrupt changes of orography in the world. Therefore, the same type of works could be also performed in other regions of the globe that are well-known important sources of orographic GW. Given the present scarce observational information of GWMF around the world and at different heights, the development of other similar studies may prove to be useful for GCM parameterizations improvements. Advances in this subject must rely on the coming observational contributions, but also on numerical and theoretical progress. Understanding the detailed mechanisms responsible for the possible change of the GWD in the future requires further investigation, which is out of the scope of the present work. However, our results highlight the need for its adequate representation in numerical models of the present and the future.

Acknowledgements

Manuscript prepared under Grants UBA X004 and CONICET PIP 5932 and ANPCYT PICT 1999. P. Alexander and C. Menéndez are members of CONICET. A.A. Sörensson has a grant from Rossby Centre, Swedish Meteorological and Hydrological Institute (SMHI). This work was begun while A.A. Sörensson visited SMHI in Norrköping, Sweden, invited by Rossby Centre and with financial

support from SMHI. The model simulations were made on the climate computing resource Tornado funded with a grant from the Knut and Alice Wallenberg foundation. Thanks to Ulf Hansson for technical support. We acknowledge data provided by the Rossby Centre.

References

Alexander, M.J. Interpretations of observed climatological patterns in stratospheric gravitywave variance. J. Geophys. Res. 103, 8627–8640, 1998.

Alexander, P., Luna, D., Llamedo, P., de la Torre, A. A gravity waves study close to the Andes mountains in Patagonia and Antarctica with GPS radio occultation observations. Ann. Geophys. 28, 587–595, 2010.

Andrews, D.G., Holton, J.R., Leovy, C.B. Middle Atmosphere Dynamics p. 489, 1987. Academic Press, Orlando, 2010.

Bacmeister, J.T., Schoeberl, M.R., Lait, L.R., et al. ER-2 Mountain wave enconter over Antarctica: evidence for blocking. Geophys. Res. Lett. 17, 81–84, 1990.

Bacmeister, J.T., Eckermann, S.D., Newman, P.A., et al. Stratospheric horizontal wavenumber spectra of winds, potential temperature, and atmospheric tracers observed by high-altitude aircraft. J. Geophys. Res. 101, 9441–9470, 1996.

Baines, P.G. Topographic Effects in Stratified Fluids p. 482, 1995. Cambridge University Press, New York, 1996.

Chen, C.-C., Durran, D.R., Hakim, G.J. Mountain-wave momentum flux in an evolving synoptic-scale flow. J. Atmos. Sci. 62, 3213–3231, 2005.

de la Torre, A., Alexander, P. Gravity waves above Andes detected from GPS radio occultation temperature profiles: mountain forcing? Geophys. Res. Lett. 32, L17815, doi:10.1029/2005GL022959, 2005.

de la Torre, A., Alexander, P., Llamedo, P., et al. Recent advances in gravity wave analysis from long term global GPS radio occultation observations, in: New Horizons in Occultation Research. Springer-Verlag, Berlin, p. 316, 2009.

Eckermann, S.D., Preusse, P. Global measurements of tratopheric mountain waves from space. Science 286, 1534–1537, 1999.

Ern, M., Preusse, P., Alexander, M.J., Warner, C.D. Absolute values of gravity wave momentum flux derived from satellite data. J. Geophys. Res. 109, D20103, doi:10.1029/2004JD004752, 2004.

Eyring, V., Waugh, D.W., Bodeker, G.E., et al. Multimodel projections of stratospheric ozone in the 21st century. J. Geophys. Res. 112, D16303, doi:10.1029/2006JD008332, 2007.

Fetzer, E.J., Gille, J.C. Gravity wave variance in LIMS temperatures. Part I: variability and comparison with background winds. J. Atmos. Sci. 51, 2461–2483, 1994.

Forster, P.M., Shine, K.P. Assessing the climate impact and its uncertainty for trends in stratospheric water vapor. Geophys. Res. Lett. 29, doi:10.1029/2001GL01390, 2002.

Fritts, D.C., Alexander, J. Gravity wave dynamics and effects in the middle atmosphere. Rev. Geophys. 41, 1003, doi:10.1029/2001RG000106, 2003.

Garcia, R.R., Randel, W.J. Acceleration of the Brewer–Dobson circulation due to increases in greenhouse gases. J. Atmos. Sci. 65, 2731–2739, 2008.

Gill, A. Atmosphere–Ocean Dynamics p. 645, 1982. Academic Press, New York, 2008.

Hamming, R.W. Digital Filters, third ed Dover Publications, Mineola, 1998.

Hines, C.O. Internal atmospheric gravity waves at ionospheric heights. Can. J. Phys. 38, 1441–1481, 1960.

Hong, S.-Y., Choi, J., Chang, E.-C., et al. Lower tropospheric enhancement of gravity wave drag in a global spectral atmospheric forecast model. Weather Forecast. 23, 523–531, 2008.

Jungclaus, J.H., Keenlyside, N., Botzet, M., et al. Ocean circulation and tropical variability in the coupled model ECHAM5/MPI-OM. J. Climate 19, 3952–3972, 2006.

Kim, Y.J., Eckermann, S.D., Chun, H.Y. An overview of the past, present, and future of gravity-wave drag parameterization for numerical climate and weather prediction models. Atmos. Ocean 41, 65–98, 2003.

Kjellström, E., Bärring, L., Gollvik, S., et al., A 140-year simulation of European climate with the new version of the Rossby Centre regional atmospheric climate model (RCA3), Reports meteorology and climatology No. 108, SMHI, SE-60176 Norrkping, Sweden, p. 54, 2005.

Lappen, C.L., Randall, D.A. Toward a unified parameterization of the boundary layer and moist convection. Part I: a new type of mass-flux model. J. Atmos. Sci. 58, 2021–2036, 2001.

Li, F., Austin, J., Wilson, J. The strength of the Brewer–Dobson circulation in a changing climate: coupled chemistry-climate model simulations. J. Climate 21, 40–57, 2008.

Lindzen, R. Wave-mean flow interactions in the upper atmosphere. Boundary Layer Meteorol. 4, 327–343, 1973.

Lott, F., Miller, M.J. A new subgrid-scale orographic drag parametrization: its formulation and testing. Q. J. R. Meteorol. Soc. 123, 101–127, 1997.

Lovejoy, S., Tuck, A.F., Hovde, S.J., Schertzer, D. Vertical cascade structure of the atmosphere and multifractal dropsonde outages. J. Geophys. Res. 114, D07111, doi:10.1029/2008JD010651, 2009.

Marengo, J.A., Jones, R., Alves, L.M., Valverde, M.C. Future change of precipitation and temperature extremes in South America as derived from the PRECIS regional climate modeling system. Int. J. Climatol., doi:10.1002/joc.1863, 2009.

McFarlane, N.A. The effect of orographically excited gravity-wave drag on the general circulation of the lower stratosphere and troposphere. J. Atmos. Sci. 44, 1775–1800, 1987.

McLandress, C., Shepherd, T.G. Simulated anthropogenic changes in the Brewer–Dobson circulation, including its extension to high latitudes. J. Climate 22, 1516–1540, 2009.

Nappo, C.J. An Introduction to Atmospheric Gravity Waves. Academic Press, San Diego, 2002.

Palmer, T.N., Shutts, G.J., Swinbank, R. Alleviation of a systematic westerly bias in general circulation and numerical weather prediction models through an orographic gravity wave drag parametrization. Q. J. R. Meteorol. Soc. 112, 1001–1039, 1986.

Pierrehumbert, R.T., Wyman, B. Upstream effects of mesoscale mountains. J. Atmos. Sci. 42, 977–1003, 1985.

Preusse, P., Eckermann, S.D., Offermann, D. Comparison of global distributions of zonal-mean gravity wave variance inferred from different satellite instruments. Geophys. Res. Lett. 27, 3877–3880, 2000.

Preusse, P., Dörnbrack, A., Eckermann, S.D., et al. Space based measurements of stratospheric mountain waves by CRISTA: 1. Sensitivity, analysis method, and a case study. J. Geophys. Res. 107, 8178, doi:10.1029/2001JD000699, 2002.

Preusse, P., Eckermann, S.D., Ern, M. Transparency of the atmosphere to short horizontal wavelength gravity waves. J. Geophys. Res. 113, D24104, doi:10.1029/2007JD009682, 2008.

Rind, D., Suozzo, R., Balachandran, N.K., Prather, M.J. Climate change and the middle atmosphere. 1: the doubled CO_2 climate. J. Atmos. Sci. 47, 475–494, 1990.

Roeckner, E., Bäuml, G., Bonaventura, L., et al. The atmospheric general circulation model ECHAM5. Part I: model description, Rep. 349, Max–Planck–Institut fr Meteorologie, Hamburg, p. 127, 2003.

Rontu, L. Studies on Orographic Effects in a Numerical Weather Prediction Model No. 63, p. 61, 2007. Finish Meteorological Institute, Helsinki, 2003.

Scinocca, J.F., McFarlane, N.A. The parameterization of drag induced by stratified flow over anisotropic orography. Q. J. R. Meteorol. Soc. 126, 2353–2393, 2000.

Shutts, G.J., Kitchen, M., Hoare, P.H. A large amplitude gravity wave in the lower stratosphere detected by radiosonde. Q. J. R. Meteorol. Soc. 114, 579–594, 1988.

Sigmond, M., Scinocca, J.F., Kushner, P.J. Impact of the stratosphere on tropospheric climate change. Geophys. Res. Lett. 35, L12706, doi:10.1029/2008GL033573, 2008.

Sigmond, M., Scinocca, J.F. The influence of the basic state on the Northern Hemisphere circulation response to climate change. J. Climate 23, 1434–1446, 2010.

Smith, R.B. Stratified flow over topography, in: Grimshaw, R. (Ed.), Environmental Stratified Flows. Kluwer, London, pp. 121–159, 2001.

Solomon, S., Rosenlof, K.H., Portmann, R.W., et al. Contributions of stratospheric water vapor to decadal changes in the rate of global warming. Science 327, 1219–1223, 2010.

Sörensson, A.A., Menéndez, C.G., Ruscica, R., et al. Projected precipitation changes in South America: a dynamical downscaling within CLARIS. Meteorol. Z. 19, 347–355, 2010.

Stein, J. Investigation of the regime diagram of hydrostatic flow over a mountain with a primitive equation model. Part I: twodimensional flows. Mon. Weather Rev. 120, 2962–2976, 1992.

Tsuda, T., Nishida, M., Rocken, C., Ware, R.H. A global morphology of gravity wave activity in the stratosphere revealed by the GPS occultation data (GPS/MET). J. Geophys. Res. 105, 7257–7273, 2000.

Walterscheid, R.L. Gravity wave transports and their effects on the large-scale circulation of the upper mesosphere and lower thermosphere. Adv. Space Res. 27, 1713–1721, 2001.

Webster, S., Brown, A.R., Cameron, D.R., Jones, C.P. Improvements to the representation of orography in the met office unified model. Q. J. R. Meteorol. Soc. 129, 1989–2010, 2003.

Wu, D.L., Waters, J.W. Satellite observations of atmospheric variances: a possible indication of gravity waves. Geophys. Res. Lett. 23, 3631–3634, 1996.

Wu, D.L. Mesoscale gravity wave variances from AMSU-A radiances. Geophys. Res. Lett. 31, L12114, doi:10.1029/2004GL019562, 2004.

Wu, L.D., Preusse, P., Eckermann, S.D., et al. Remote sounding of atmospheric gravity waves with satellite limb and nadir techniques. Adv. Space Res. 37, 2269–2277, 2006.

Zülicke, C., Peters, D. Simulation of inertia-gravity waves in a poleward-breaking Rossby wave. J. Atmos. Sci. 63, 3253–3276, 2006.